ChemSusChem

Research Article
doi.org/10.1002/cssc.202102434

Chemistry Europe
European Chemical Societies Publishing

www.chemsuschem.org

VIP *Very Important Paper*

Modulating the Coupling Efficiency of P450 BM3 by Controlling Water Diffusion through Access Tunnel Engineering

Shuaiqi Meng[+],[a] Yu Ji[+],[a] Luo Liu,[b] Mehdi D. Davari,[c] and Ulrich Schwaneberg*[a, d]

Cytochromes P450 have gained much interest for their broad substrate scope in the catalysis of oxidation reactions for pharmaceuticals, plastics, and hormones. However, achieving high coupling efficiency by the engineering of P450s is still a big challenge. The presence of extra water around the active site is deemed to be related to uncoupling. In this study, the access tunnels of P450 BM3 from *Bacillus megaterium* are engineered to control water access from bulk solvent to the active site. Nine residues located in tunnels are investigated by site-saturation mutagenesis to reduce water diffusion, thereby improving the coupling efficiency. The recombined variant N319L/T411V/T436A shows improved coupling efficiency (from 31.2% to 52.6%). Tunnel polarity analysis and molecular dynamics simulation further indicate that reduced water molecules around the active site lead to higher coupling efficiency. Overall, this study provides valuable insight on improving coupling efficiency by controlling water diffusion through tunnel engineering.

Introduction

Cytochrome P450 monooxygenases are a valuable enzyme superfamily, which catalyzes a broad range of reactions in chemical industry, such as hydroxylation, epoxidation, dealkylation, and sulfoxidation.[1] Biosynthesis of chemicals by P450s is a green method that reduces the usage of organic solvents leading to more sustainable production. P450s can functionalize inert C–H bonds with high regioselectivity and stereoselectivity under mild conditions, which is usually challenging in chemical synthetic routes.[2] The typical P450 catalytic cycle follows the "oxygen rebound mechanism" for hydroxylation of products (Figure 1).[3] Two electrons form NAD(P)H cofactor and two protons are transferred to the P450's heme domain via a redox partner to active the P450 and oxidize the target substrate.

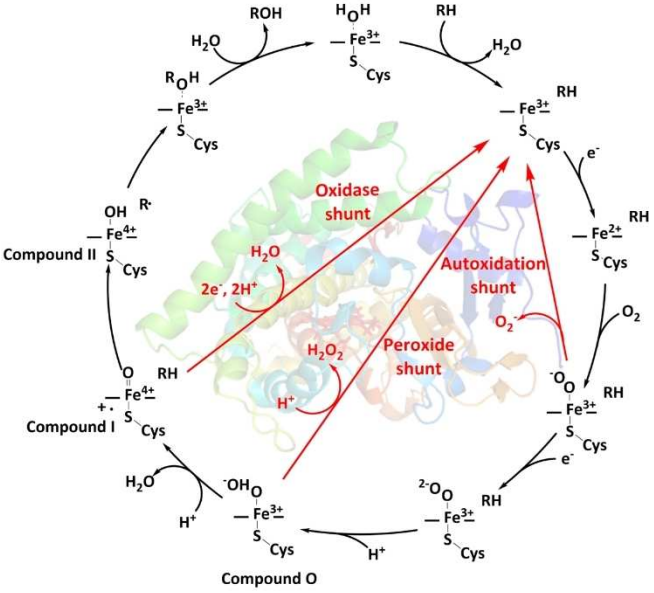

Figure 1. Cytochrome P450 catalytic cycle. This figure is redrawn with reference to the P450 catalytic diagram by Grinkova et al.[3b] and Grivan and Munro.[3a] The canonical P450 catalytic cycle is shown with black arrows. Uncoupling pathways are shown with red arrows.

However, the consumption of NAD(P)H is not always stoichiometric in accordance with the formed products.[4] Coupling efficiency describes the utilization efficiency of NAD(P)H, which represent the ratio of formed products to consumed NADPH. Generally, P450s have high coupling efficiency (close to 100%) to its natural substrate (e.g., lauric acid).[5] Unfortunately, the coupling efficiency is often low with nonnatural substrates.[5a] For example, the coupling efficiency is only 14% for benzene, 8.8% for benzo-1,4-dioxane, and 0.5% for cetyl trimethylammonium bromide with P450 BM3 as catalyst.[6] Uncoupling

[a] S. Meng,[+] Dr. Y. Ji,[+] Prof. U. Schwaneberg
Institute of Biotechnology, RWTH Aachen University
Worringerweg 3, 52074 Aachen (Germany)
E-mail: u.schwaneberg@biotec.rwth-aachen.de
[b] Prof. L. Liu
Beijing Bioprocess Key Laboratory, Beijing University of Chemical Technology
Beisanhuan East Road 15, Beijing 10029 (P. R. China)
[c] Dr. M. D. Davari
Department of Bioorganic Chemistry, Leibniz Institute of Plant Biochemistry
Weinberg 3, 06120 Halle (Germany)
[d] Prof. U. Schwaneberg
DWI-Leibniz Institute for Interactive Materials
Forckenbeckstraße 50, 52074 Aachen (Germany)
[+] These authors contributed equally to this work.

Supporting information for this article is available on the WWW under https://doi.org/10.1002/cssc.202102434

This publication is part of a collection of invited contributions focusing on "Biocatalysis as Key to Sustainable Industrial Chemistry". Please visit chemsuschem.org/collections to view all contributions.

© 2021 The Authors. ChemSusChem published by Wiley-VCH GmbH. This is an open access article under the terms of the Creative Commons Attribution Non-Commercial NoDerivs License, which permits use and distribution in any medium, provided the original work is properly cited, the use is non-commercial and no modifications or adaptations are made.

© 2021 The Authors. ChemSusChem published by Wiley-VCH GmbH

often leads to the inefficient use of expensive NAD(P)H cofactors and cause the accumulation of reactive oxygen species, represented by superoxide anion and hydrogen peroxide (H_2O_2), which is toxic oxidant that damages the organisms.[4,7] Most studies have focused on improving catalytic performance. Generally, the increased coupling efficiency is accompanied by increased catalytic performance. However, the coupling efficiency and the catalytic performance are not identical. Coupling efficiency determines the consumption efficiency of the cofactor NADPH, whereas catalytic performance is regulated by many factors, including coupling efficiency. As a result, the two concepts are not fully synchronized but are positively correlated. There are many works dedicated to improving coupling efficiency. For example, Dominique et al. engineered the electrons transfer pathways of P450 BM3, resulting in a 32-fold improvement in coupling efficiency.[4] Hoffmann et al. studied the linker region between CYP153 and reductase PFOR.[8] By increasing the linker by two amino acids, they obtained L3 variant with improved coupling efficiency (from 39% to 94%). However, how to develop new strategies for improving coupling efficiency is still one of the main challenges in P450s engineering.[5a]

The uncoupling mechanism has been suggested for three pathways (Figure 1).[3b,9] The first uncoupling reaction occurs after the dioxygen binding. Inappropriate second electronic transmission could lead to lost superoxide (autoxidation shunt).[10] Secondly, if a substrate position in the active site in an catalytically incompetent orientation, the protonation of ferric hydroperoxo intermediates (compound O) could lead to hydrogen peroxide formation (peroxide shunt).[10] Thirdly, the compound I state could receive extra electrons and protons resulting in the water formation (oxidase shunt).[10] Among the three uncoupling pathways, the autoxidation shunt is relatively slow and not usually involved in the uncoupling reaction, while the other two pathways contribute to the major of uncoupling.[9] The peroxide shunt and oxidase shunt are regarded to be related with presence of extra water around the active site. Residual water in active site would provide protons during catalysis process could destabilize iron-oxo species, leading to the formation of H_2O_2 and H_2O.[9,11] The X-ray structure of CYP101 showed presence of residual water in the active site with non-natural substrate, but no water presence in active site with CYP101's natural substrate camphor.[12] MD simulations on CYP154C5 variants also proved that more water entrancing the active site would cause higher uncoupling.[13] Hence, controlling the water access to the active site could be a promising way for improved the coupling efficiency of P450s.

The critical problem we are now facing is how to control the water diffusion to the active site of P450s. Cytochrome P450s have an active site buried deeply inside the enzyme near the heme cofactor.[14] During P450s' catalytic process, the transportation of substrates, products, and water to and out of the active site rely on the tunnels connecting enzyme internal cavities and bulk solvent environment. Although part of tunnels is involved in the binding pocket, most of them do not belong to the active site.[15] Therefore, reengineering of tunnels could provide a strategy for improving coupling efficiency without interference of common P450 reaction.

In this study, P450 BM3 (CYP102A1) from *Bacillus megaterium*, which is the best-characterized enzyme among the P450 family, was chosen to investigate tunnel engineering for improved coupling efficiency. The oxidation of α-isophorone was selected as model reaction because of the industrial value of 4-hydroxyisophorone and ketoisophorone which are important for vitamin E production (Figure S1 in the Supporting Information).[16] In the present study, 9 residues (N70, S72, L181, D182, H266, N319, S332, T411, and T436) located in the P450 BM3 access tunnels were identified for controlling water access by computational analysis and therefore single site saturation mutagenesis (SSM) was carried for positions H266, N319, S332, T411, and T436 and double-site-simultaneous mutagenesis was carried for positions N70/S72 and L181/D182. After screening these seven libraries, beneficial substitutions were identified and analyzed in silico to understand the improvement in coupling efficiency by tunnel engineering.

Results and Discussion

The results and discussion parts are divided into three parts to illustrate how to control the P450 BM3 coupling efficiency by tunnel engineering. In the first part, the access tunnels of P450 BM3 were analyzed, and nine potential functional residues were selected. The second part describes the library generation and screening results. Additionally, the beneficial variants were further characterized. In the third part, we recombined the beneficial substitutions and further analysis how the mutagenesis influences the P450 BM3 coupling efficiency by increasing the tunnel hydrophobicity.

Analysis of access tunnels and identification of key residues

P450 BM3 has active sites buried in the center of enzyme next to the heme cofactor and the access tunnels connect the active site and solvent environment, performing important functions for controlling the entry of the substrate and water.[14a] As excess of water accessing to the distal binding pocket of heme domain contributes to uncoupling in P450 BM3,[9] analyzing the access tunnels for monitoring the water diffusion could provide an understanding in fine tuning of coupling efficiency. Five access tunnels of wild-type P450 BM3 were identified using CAVER Web 1.0 server[17] based on crystal structure (PDB: 1BU7) (Figure 2 and Table S2). Tunnel 1–4 may involve substrate and water exchange because of the short length and the wide bottleneck while Tunnel 5 was identified as putative water tunnel as this tunnel was not observed as transport pathway for substrates or products (Table S2).[14a] Given that, all five tunnels were investigated in this study to gain a comprehensive knowledge.

A total of 88 residues are considered to be involved in the construction of the access tunnels of P450 BM3 (Table S3) based on CAVER Web 1.0 server. To identify key residues, three

© 2021 The Authors. ChemSusChem published by Wiley-VCH GmbH

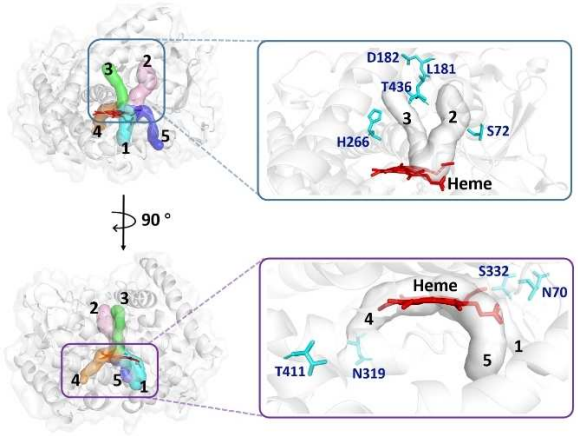

Figure 2. Access tunnels and selected residues in wild-type P450 BM3 (PDB: 1BU7[20]) for tunnel engineering. Two orientations of P450 BM3 (90 degree rotation) are shown for clarity. CAVER Web 1.0 server[17] was used for tunnel identification and five tunnels were identified (tunnel 1: cyan; tunnel 2: pink; tunnel 3: green; tunnel 4: orange; tunnel 5: blue). Nine amino acid residues targeted for site-saturation mutagenesis are shown in cyan.

criterions (hydrophobicity analysis, tunnel bottleneck analysis, and evolutionary conservation analysis) were evaluated. To avoid the entering of excess water to the active site, 18 hydrophilic residues located in the bottleneck of access tunnels were preliminarily selected (Table S3). Meanwhile, an evolutionary conservation analysis was carried out by the ConSurf server to exclude the conserved functional and structural residues (Figure S3) in order to avoid the enzyme inactivation or misfolding. Overall, seven potential positions (70, 72, 182, 319, 332, 411, and 436) were selected as mutational targets (Figure 2). In addition, position 266 and 181 located in the tunnel bottleneck identified by Anna *et.al* which could influence the entrance of water to the active site was also targeted for mutagenesis.[18] Among these nine residues, S72, S332, and T436 were located on the edge of putative hydrophobic substrate pocket, while other residues were located far away from the active site (Figure S2). Those residues could exert more influence on substrate and water transportation rather than the direct influence on the transition state in catalytic process. The substitution stability of these nine positions was separately evaluated by analysis of the relative free energy of folding ($\Delta\Delta G_{fold}$), which was employed to evaluate the intrinsic stability of mutagenesis.[19] Most of the substitutions showed no obvious instability ($\Delta\Delta G_{fold} > 7.52$ kcal mol^{-1},Table S6) and could be mutated.[19] For adjacent positions (position 70/72 and 181/182), we did the double site simultaneous mutagenesis to explore the synergy effect. Finally, five individual SSM libraries (SSM266, SSM319, SSM332, SSM411, and SSM436) and two double site saturation mutation libraries (SSM70/72 and SSM181/182) were generated. All individual SSM libraries contained 192 colonies and all double site SSM libraries contained 960 colonies for further screening.

Library screening and characterization of beneficial variants

α-Isophorone was chosen as the model substrate as the importance of the 4-hydroxyisophorone and ketoisophorone product within vitamin E synthesis.[16,21] It is expected to obtain improve P450 BM3 coupling efficiency while maintaining activity. The saturation mutagenesis libraries were screened and rescreened using NADPH consumption assay in MTPs and the best five variants from each library were selected for sequencing (Table S5). Subsequently, 16 variants were selected for further expression in flask and characterization under a normalized enzyme concentration. As a general trend, the NADPH consumption rate of best variants from libraries SSM319, SSM332, SSM411, SSM436, and SSM70/72 have slightly improvement compared to wild-type P450 BM3 (0.93–2.23-fold improvement; Figure 3). However, the variants from SSM266 and SSM181/182 libraries showed significantly increased NADPH consumption rate (9.32/8.86-fold improvement; Figure 3). Surprisingly, in library SSM332, all five best variants were replaced by serine, which indicated the S332 should be a key residue in α-isophorone oxidation. It was reported that S332 is involved in the stabilization of substrate binding by H bond, which was also observed in one binding pose by our molecular docking analysis (Figure S4).[22] In total 16 substitutions were selected from all SSM libraries (5 substitutions from library SSM181/182, 3 substitutions from library SSM266, and 2 substitutions from SSM319, SSM411, SSM436 and SSM70/72; Figure 3) and the coupling efficiency of each variant was investigated using GC-MS and spectrophotometer (Table S7). Six variants (N319A, N319L, T411A, T411V, T436A, and T436Q) showed improved coupling efficiency comparable to wild-type P450 BM3 (from 1.15-fold to 1.38-fold, Table S7), which were selected for kinetic characterization. The variants from SSM266 and SSM181/182 showed high NADPH consumption rate, but the coupling efficiency were not as high as wild-type P450 BM3. A representative example is H266T substitution, which showed a 9.3-fold higher NADPH consumption rate but a 2.5-fold

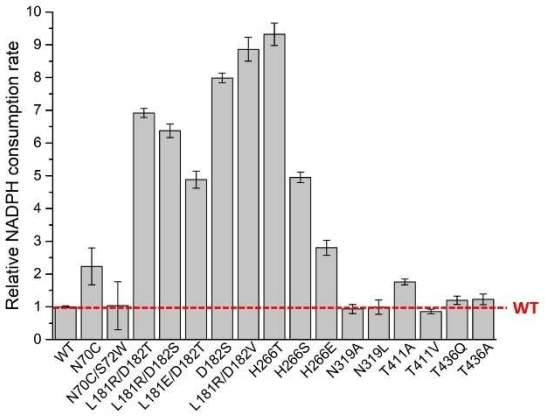

Figure 3. Relative NADPH consumption rates of wild-type P450 BM3 and its variants obtained from seven SSM libraries. The relative NADPH consumption rate of wild-type P450 BM3 was set to 1. Measurements were performed in triplicate.

© 2021 The Authors. ChemSusChem published by Wiley-VCH GmbH

decrease in coupling efficiency compared with wild-type P450 BM3.

Recombination and mechanism analysis

The beneficial substitutions were combined based on the CompassR rule to investigate the synergy effect of substitutions further.[19] N319L, T411V, and T436A substitutions were selected for further recombination because of their lower relative free energy of folding [$\Delta\Delta G_{fold}$(N319L) = −1.56 kcal mol^{-1}, $\Delta\Delta G_{fold}$(T411V) = −0.05 kcal mol^{-1}, $\Delta\Delta G_{fold}$(T436A) = 2.43 kcal mol^{-1}; Table S6], which indicated those substitutions are more stable. Three double mutations (N319L/T411V, N319L/T436A and T411V/T436A) and one triple mutation (N319L/T411V/T436A) were selected for purification and characterization. All four variants showed improved coupling efficiency (from 1.59-fold to 1.69-fold; Table 1) and variant N319L/T411V/T436A showed the highest coupling efficiency (52.56%) among all the variants. Obviously, compared with wild-type P450 BM3, the replacement of hydrophilic amino acids (e.g., asparagine and threonine) to hydrophobic amino acids (e.g., alanine, leucine, and valine) benefits to improved coupling efficiency.

To investigate the tunnel hydrophobicity, beneficial variants was analyzed using MOLEonline server (Figure S5).[23] The polarity of tunnel 3 was decreased by substitutions on T436 (Figure 4a and Table S9) while the polarity of tunnel 4 was significantly reduced by substitutions on 319 and T411 (Figure 4b and Table S9). The recombined variants (N319L/T436A, T411V/T436A, N319L/T411V/T436A) affect both tunnel 3 and tunnel 4 (Figure 4a,b, Table S9). In particular, after substitution of position 319, 411 and 436 (e.g., N319L/T411V/T436A), the entrance of tunnel 3 and 4 shows significant reduction (Figure 4c and Figure S7), which could inhibit the water access from solvent environment to P450 BM3 active site. Interestingly, substitution T436Q also showed decreased tunnel polarity, although glutamine is more hydrophilic than threonine.[24] By visualization the 3D structure of P450 BM3, substitution T436Q moved out from tunnel 3 compared with WT (Figure S6), while an extra non-polar residue (P170) is involved in tunnel 3. The moving of position 436 in variant T436Q may be due to the longer side chain of glutamine than the side chain of threonine. The results shows that introduction of hydrophilic amino acids could also affect the tunnel structure, resulting in increased hydrophobicity of P450 BM3 access tunnels.

The best variant N319L/T411V/T436A (coupling efficiency: 52.56%) also showed 1.44-fold improved catalytic efficiency (k_{cat}/K_M) compared to wild-type P450 BM3 (from 66.7 to 95.8 L mol^{-1} s^{-1}, Table 1). The comparison between BM3 WT and the variant N319L/T411V/T436A was shown in Figure S8. Overall, the structure of BM3 WT showed high similarity with the variant N319L/T411V/T436A with the RMSD of 0.424 Å on alpha carbons (Figure S8a). Based on the structure alignment, a main difference appeared in the loop 432–441 of WT and variant N319L/T411V/T436A. Compared with WT, the loop in variant N319L/T411V/T436A was determined with an offset of 1 Å, which cause the tunnel to be closer to be hydrophobic A436 residue in variant N319L/T411V/T436A (Figure S8a,b). By contrast, residues 319 and 411 residues are located on the α-helix region. Substitution of the two residues did not cause obvious structural changes.

To further explore the molecular mechanism of the effect of water, the molecular dynamics (MD) simulation was carried out. To evaluate the substrate flexible, root mean square fluctuations (RMSF) of α-isophorone substrate was investigated. The RMSF of α-isophorone in variant N319L/T411V/T436A showed a similar value with wild-type P450 BM3 (Figure S11) and α-isophorone in variant N319L/T411V/T436A appear as stable in wild-type P450 BM3. The positions (319, 411, and 436) far away from the active site seems not affect the compatibility between α-isophorone and P450 BM3 active site. The average number of water molecules within 1 nm of heme iron showed a significant reduction (17%) in variant N319L/T411V/T436A compared to wild-type P450 BM3 during MD simulation (Figure 5a). In addition, comparing the water distribution around the heme molecular, it is also observed that the water distribution of N319L/T411V/T436A variant showed lower than the water distribution of wild-type P450 BM3 (Figure 5b–d). In short, variant N319L/T411V/T436A could reduce the diffusion of water to the active site, thereby resulting in a higher coupling efficiency.

The water condition around heme iron also can be reflected in heme iron spin state.[25] As the substrate binds, the coordinated water molecule is expelled from the active site, inducing the spin stage of heme iron from low spin to high spin.[25] The UV/Vis spectroscopy for P450 BM3 WT and variant N319L/T411V/T436A with substrate of α-isophorone showed in Figure 6. The high spin ferric heme and low spin ferric heme was characterized by the peak at 390 nm and 420 nm, respectively. Both WT and variant N319L/T411V/T436A showed

Table 1. The coupling efficiency and kinetic parameters of P450 BM3 wild type and variants.

P450 BM3	Coupling efficiency [%]	Conversion [%][a]	Kinetic parameters		
			K_M [mmol L^{-1}]	k_{cat} [s^{-1}]	k_{cat}/K_M [L mmol^{-1} s^{-1}]
Wild type	31.18 ± 0.96	11.96 ± 0.70	10.95 ± 0.80	0.72 ± 0.05	66.7
N319L/T411V	49.70 ± 1.17	18.73 ± 0.90	17.67 ± 0.46	0.95 ± 0.03	53.6
N319L/T436A	51.64 ± 1.46	16.39 ± 0.46	10.09 ± 0.18	0.80 ± 0.13	79.3
T411V/T436A	49.77 ± 3.37	17.77 ± 2.06	11.39 ± 0.84	0.86 ± 0.12	75.6
N319L/T411V/T436A	52.56 ± 2.37	20.13 ± 0.91	8.29 ± 0.77	0.79 ± 0.08	95.8

[a] Conversion was determined with 3 μM purified P450 BM3 monooxygenase, 20 mM α-isophorone, 300 mM glucose, 4 U mL^{-1} GDH, 200 U mL^{-1} catalase, 500 μM NADP$^+$, and KPi (50 mM, pH 7.4) in a total volume of 1 mL. The reactions were performed at 30 °C for 22 h. Measurements were performed in triplicate.

© 2021 The Authors. ChemSusChem published by Wiley-VCH GmbH

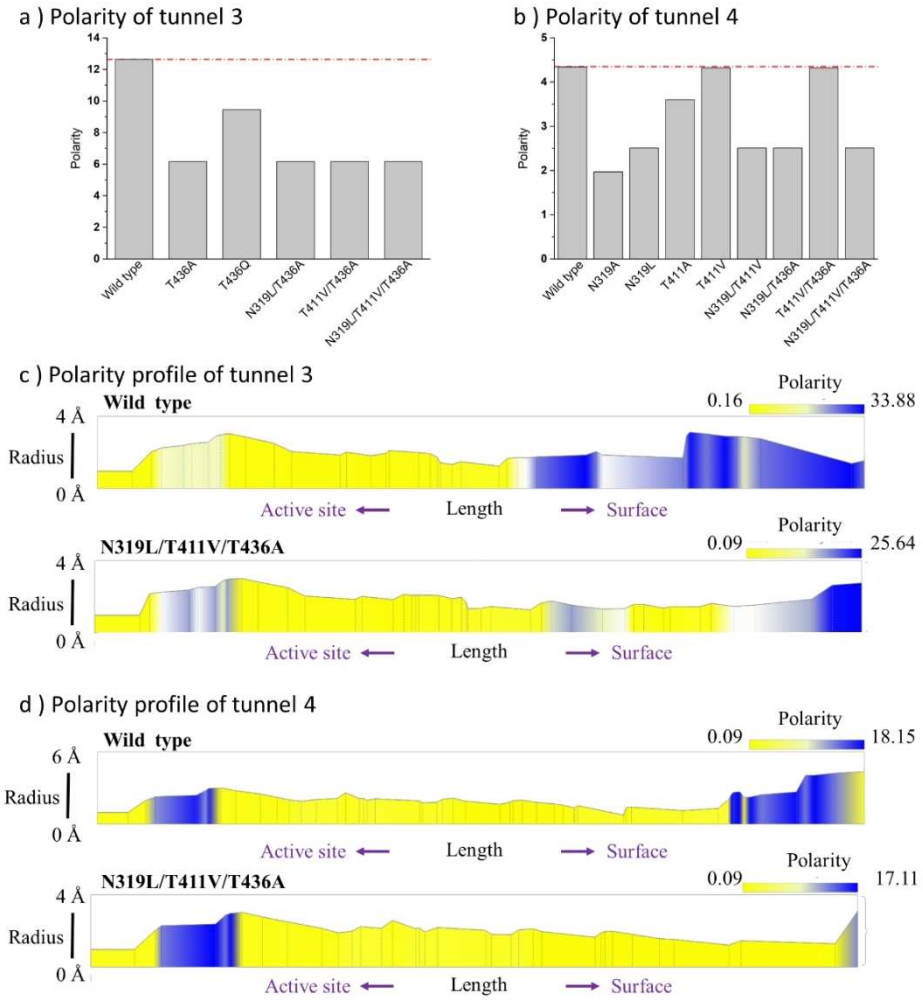

Figure 4. Analysis of tunnel polarity of wild-type P450 BM3 and its variants: a,b): Polarities of tunnel 3 and tunnel 4 in wild-type P450 BM3 and its variants with improved coupling efficiency. c,d): Polarity profiles of tunnels 3 and tunnel 4 in wild-type P450 BM3 and N319L/T411V/T436A variant. Tunnel polarities were calculated by MOLEonline server. The polarity index accord to the scales by Zimmerman et al. from nonpolar (e.g., Ala, Gly = 0), through polar (e.g., Ser = 1.67), to charged (e.g., Glu = 49.90, Arg = 52.00).[24]

mixed spin states on the addition of saturating concentration of substrate of α-isophorone (Figure 6a). It is evident that the variant N319L/T411V/T436A have more high spin stage of heme iron, which indicate the engineered variant contained less extra water molecule at the active site than the WT. In addition, the apparent dissociation constants (K_d) of WT and variant N319L/T411V/T436A for α-isophorone were calculated as 6853 ± 79 μM and 6263 ± 47 μM (Figure 6b,c). Therefore, the variant N319L/T411V/T436A showed improved binding capacity with the α-isophorone than the WT.

Conclusion

A tunnel engineering strategy was used to improve of the coupling efficiency of P450 BM3. The replacements of hydrophilic residues with hydrophobic residues in P450 BM3 access tunnels decreased extra water access to the active site and led to improved coupling efficiency. The variant N319L/T411V/T436Q showed a 1.7-fold improvement in coupling efficiency (from 31.18% to 52.56%) and a 1.4-fold improvement in enzymatic activity (k_{cat}/K_M; from 66.7 L mmol^{-1} s^{-1} to 95.8 L mmol^{-1} s^{-1}) towards α-isophorone substrate compared with wild-type P450 BM3. Tunnel polarity analysis and MD simulations further proved that reducing the concentration of water molecules around the active site leads to higher coupling efficiency. These results demonstrate that tunnel engineering is a powerful strategy to control water diffusion and tune the coupling efficiency of P450s.

Experimental Section

Strain, plasmid, and chemicals

The wild-type P450 BM3 gene from *Bacillus megaterium* (NCBI Reference Sequence WP_034650526.1) and all mutants were cloned into expression vector pALXtreme-1a (derived pET-28a(+) vector).[6b] *Escherichia. coli* BL21(DE3) lacI^{Q1} strain was used for heterologous

© 2021 The Authors. ChemSusChem published by Wiley-VCH GmbH

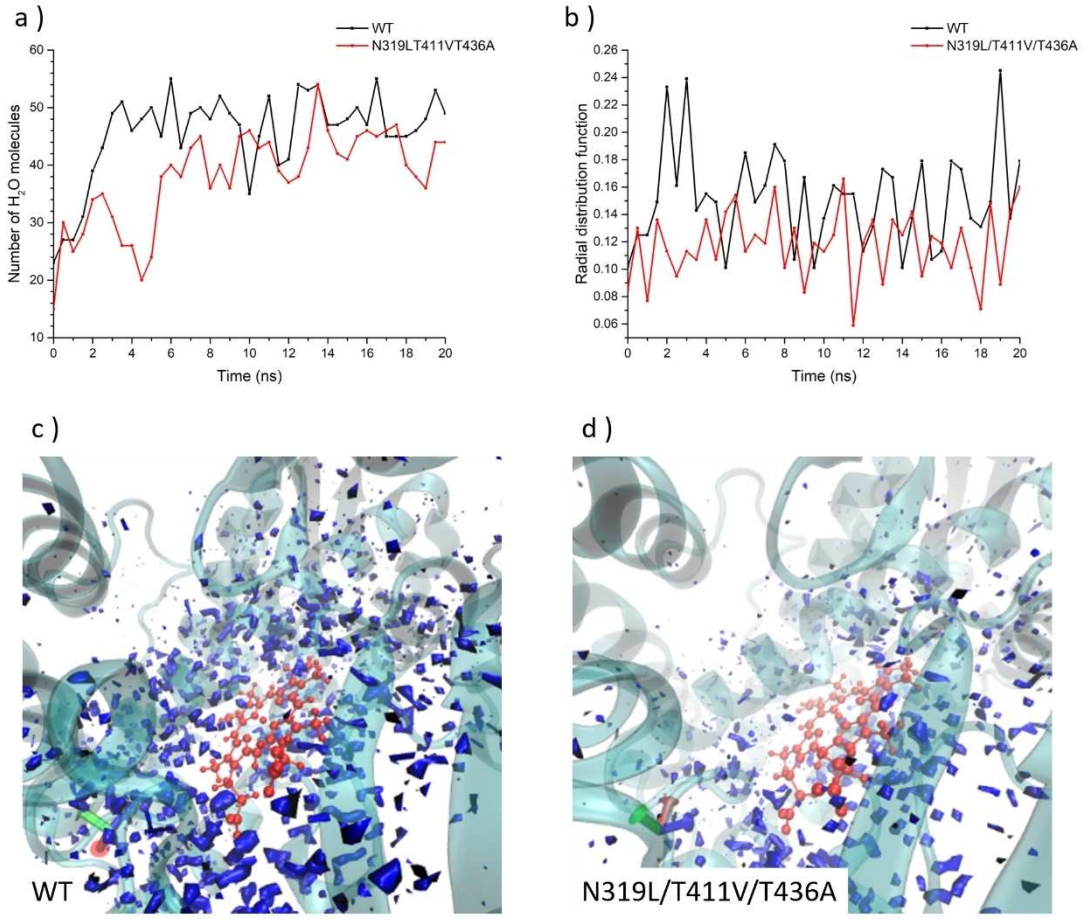

Figure 5. Water distribution status around the heme molecule of wild-type P450 BM3 and its variants: a,b) Changes of the number of water molecules (a) and radial distribution functions (b) of water molecules within 1 nm of heme iron during a 20 ns molecular dynamics simulation. c,d) Spatial distribution functions of water molecules around the heme cofactor of wild-type P450 BM3 (c) and variant N319L/T411V/T436A (d). The P450 BM3 structure is shown as a cyan cartoon rendering; the heme cofactor is shown in red; the water molecules are shown in blue. The contours are shown with isovalue 35.

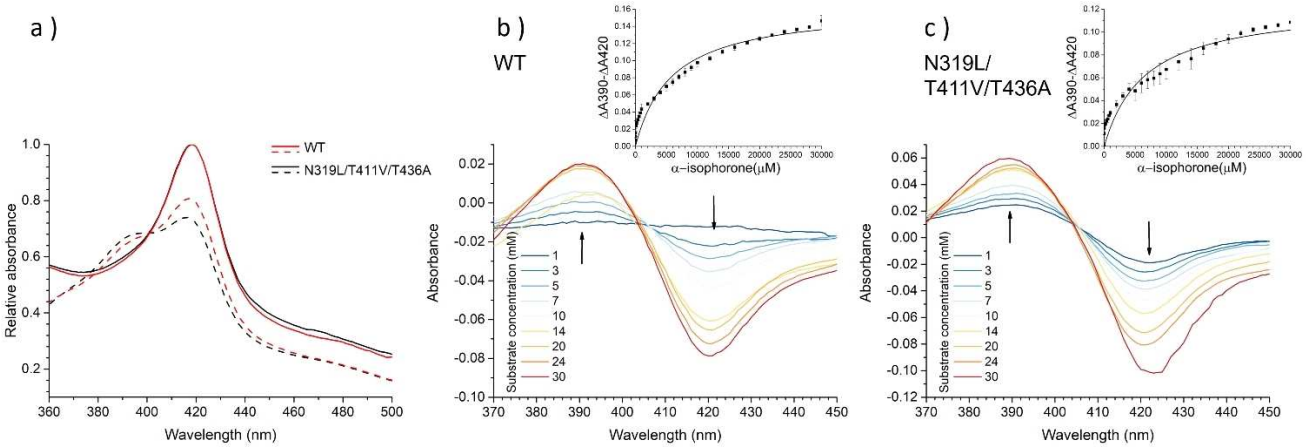

Figure 6. UV/Vis spectroscopic characterization of P450 BM3 WT and variant N319L/T411V/T436A: a) Absorption spectra of P450 BM3 WT (red line) and variant N319L/T411V/T436A (black line) with saturating concentrations of α-isophorone (30 mM, dashed line) or without α-isophorone (solid line). The relative absorption values are normalized to the maximum absorption value (at 420 nm) of WT or variant N319L/T411V/T436A in substrate-free form. b,c) Difference spectra (the starting spectrum subtracted from the subsequent traces) of P450 BM3 WT (b) and variant N319L/T411V/T436A (c). The concentration set of α-isophorone is from 1 mM to 30 mM. The inset shows the value of ($\Delta A390-\Delta A420$) relative to the change in α-isophorone concentration. The K_d values of WT and variant N319L/T411V/T436A for α-isophorone were 6853 ± 79 μM and 6263 ± 47 μM.

© 2021 The Authors. ChemSusChem published by Wiley-VCH GmbH

expression host.[6b] All chemicals were purchased from Sigma-Aldrich (Hamburg, Germany), Carl Roth (Karlsruhe, Germany) or Merck (Darmstadt, Germany), unless otherwise specified. Salt-free oligonucleotides were synthesized at HPSF purity from Eurofins MWG Operon (Ebersberg, Germany). All primers used in this study are listed in Table S1. PfuS polymerase was from our lab home-made.

Site-saturation mutagenesis

The SSM libraries of P450 BM3 were generated by one-step polymerase chain reaction (PCR) using degenerated NNK codon (N: any nucleotide; K: G or T). Every PCR mixture contained PfuS polymerase (2U), 1× PfuS buffer (10 mM Tris-HCl pH 8.9, 50 mM KCl, 2 mM $MgCl_2$, 0.1% Triton X-100), dNTP mix (0.2 mM for each nucleotide), plasmid template (20 ng), forward and reverse primers (500 nM each), and ddH_2O (up to 50 μL). The PCR condition was 98 °C for 30 s (1 cycle), 98 °C for 10 s/5 °C for 30 s/72 °C for 5 min (35 cycles), 72 °C for 10 min (1 cycle). The amplified PCR products were digested by additional 20 U DpnI restriction endonuclease for 2 h to remove DNA template. Digested PCR products were purified by the Nucleospin Extract II kit (Macherey-Nagel, Dueren, Germany) and then transformed into the chemically competent *E. coli* BL21(DE3) $lacI^{Q1}$ cells. The transformation process was repeated until adequate colonies were obtained (180 colonies for each single-site saturation mutagenesis library, 900 colonies for double-site saturation mutagenesis library).

Screening procedure for improved P450 BM3 variants

Single colonies form P450 BM3 SSM library were transferred into 96-deep well micro titer plates (MTPs; 2.2 mL polypropylene plates; Brand GmbH, Wertheim, Germany) for cultivation and expression. The P450 BM3 expression and lysate preparation were carried out using the described protocol by Nazor et al.[26] In screening step, a NADPH depletion assay was performed to obtain improved P450 BM3 variants. Each well of 96-deep well MTPs contained 30 μL cell lysate with expressed P450 BM3, 2 mM α-isophorone, 2% (*v/v*) DMSO, and KPi (50 mM, pH 7.4) in a total volume of 200 μL. MTPs were incubated at room temperature for 10 min before supplementation of 50 μL NADPH (final concentration 200 μM). NADPH consumption was measured by monitoring the absorbance at 340 nm with a Tecan Sunrise MTP reader (340 nm with interval of 10 s for 5 min; Crailsheim, Germany).

Purification procedure

P450 BM3 monooxygenase were expressed in flasks and purified by anion exchange chromatography using the established protocol.[27] An ÄKTA PrimePlus FPLC system (GE Healthcare, Menchen, Germany) equipped with a HiTrap Q HP column (5 mL, GE Healthcare, Menchen, Germany) was used for purification. Eluates were concentrated with an ultrafiltration (50 kDa cutoff, Millipore, Schwalbach, Germany) and analyzed on 10% sodium dodecyl sulfate-polyacrylamide gel electrophoresis (SDS-PAGE) gels.

Characterization of P450 BM3 variants

The shaking flasks expression of wild-type P450 BM3 and the variants were carried out using the described protocol by Nazor et al.[26] Harvested cell pellets were resuspended in KPi buffer (50 mM, pH 7.4) then homogenized by sonication for 5 min (10 s on + 10 s off, 40% amplitude, Vibra-Cell VCX-130; Sonics, Newtown, CT, USA). After centrifugation (16000 × × *g*, 30 min, 4 °C) the supernatant was filtered with a 0.22 μm filter membrane. The concentration of wild-type P450 BM3 and the variants were determined by CO difference spectroscopy using the described protocol by Omura and Sato et al. ($\varepsilon = 91\ L\,mmol^{-1}\,cm^{-1}$).[28]

Coupling efficiency: Coupling efficiency was evaluated by monitoring NADPH consumption and product formation. A reaction system contained 2 μM P450 BM3 monooxygenase, 20 mM α-isophorone, 2% (v/v) DMSO, 1 mM NADPH, and KPi (50 mM, pH 7.4) in a total volume of 1 mL. The reactions were incubated at room temperature until NADPH was fully depleted then stopped by additional 100 μL 37% (*v/v*) HCl. Formed products were subsequently analyzed by gas chromatography-mass spectrometry (GC-MS, QP2010, Shimadzu, Japan). All reactions were performed in triplicate.

Long-term conversion: Productivity of wild-type P450 BM3 and its variants towards α-isophorone was obtained from a long-term reaction with a glucose dehydrogenase (GDH) coenzyme regeneration system. A reaction system contained 3 μM P450 BM3 monooxygenase, 20 mM α-isophorone, 300 mM glucose, 4 $U\,mL^{-1}$ GDH, 200 $U\,mL^{-1}$ catalase, 500 μM $NADP^+$, and KPi (50 mM, pH 7.4) in a total volume of 1 mL. The reactions were performed at 30 °C for 22 h then stopped by additional 100 μL 37% (*v/v*) HCl. Formed products were subsequently analyzed by GC-MS. All reactions were performed in triplicate.

Kinetic characterization: Kinetic parameters determination (K_M, k_{cat}) of wild-type P450 BM3 and the variants were performed in 96-well MTPs. A reaction system contained 1 μM P450 BM3 monooxygenase, 2 to 50 mM α-isophorone, 1 mM NADPH, and KPi buffer (50 mM, pH 7.4) in a total volume of 200 μL. Initial NADPH consumption rate was recorded by monitoring the absorbance at 340 nm with a Tecan Sunrise MTP reader. All reactions were performed in triplicate. Kinetic parameters were fitted by nonlinear fitting model using OriginPro 9.1.0 software (OriginLab Corporation, Northampton, MA, USA).

Product analysis by GC-MS

Products were analyzed by a gas chromatography-mass spectrometry (GC-MS, QP2010, Shimadzu, Japan) equipped with a FS-Supreme-5MS column. Products were extracted with an equal volume of ethyl acetate supplemented with 2.6 $\mu L\,mL^{-1}$ benzyl alcohol as internal standard. After centrifugation (7000 × g, 1 min), the upper organic phase was dried by anhydrous sodium sulfate and used for GC-MS analysis. The injecting temperature was 280 °C, the injection volume was 1 μL, and the injection mode was splitless. Oven temperature was controlled initially at 100 °C, then immediately increased to 175 °C at the rate of 5 $°C\,min^{-1}$, later increased to 250 °C at the rate of 20 $°C\,min^{-1}$. The concentration of α-isophorone and corresponding products were quantitatively analyzed using calibration curves of standards.

Access tunnel analysis

The heme domain of wild-type P450 BM3 (PDB: 1BU7)[20] was used for tunnel analysis. All variants were constructed by the PyMOL mutagenesis tool based on the crystal structure of P450 BM3. For preparation of the initial structure, structure cleaning and energy minimization were carried out by Yet Another Scientific Artificial Reality Application (YASARA; version 19.12.4).[29] The access tunnels were analyzed by CAVER Web 1.0 server[17] with following parameters: 0.9 Å probe radius; 3 Å shell radius; 4 Å shell depth; 3.5 clustering threshold; the start point was the heme cofactor. Water molecules were not considered in tunnel analysis. The access tunnels were analyzed by MOLEonline[23] with following parameters: 0.9 Å bottleneck radius; 3 Å bottleneck tolerance; 0.6 max tunnel

© 2021 The Authors. ChemSusChem published by Wiley-VCH GmbH

similarity; 10 Å surface cover radius; the start point was the heme cofactor.

Evolutionary conservation analysis of P450 BM3

The evolutionary conservation of P450 BM3 residues was analyzed by the ConSurf server (https://consurf.tau.ac.il).[30] The homolog search algorithm was HMMER, and the proteins database was UNIREF-90. There were 150 sequences used for a Multiple Sequence Alignment with the alignment method of MAFFT–L-INS-i.

Relative folding free energies ($\Delta\Delta G_{fold}$) analysis

The relative folding free energies $\Delta\Delta G_{fold}$ values were calculated using FoldX employing the YASARA plugin (version 19.12.4). The initial structure of wild-type P450 BM3 was based on its crystal structure (PDB: 1BU7). FoldX parameters were temperature 298 K, pH 8, and 0.05 M ionic strength. "RepairObject" process was processed to correct the residues that have non-standard torsion angles.

Molecular dynamics (MD) simulation

The P450 BM3-α-isophorone complex obtained from molecular docking was utilized as initial structure. Molecular dynamics simulation was carried out using YASARA (version 19.12.4) using the standard macro "md_run.mrc" using the Amber 14 force field[31] for the residues, GAFF2[32] and AM1BCC[33] for the heme and TIP3P for water. The atomic partial charges were derived using the AM1BCC procedure. The P450s were centered in a 12 Å simulation cell by using a periodic boundary. The box was filled with around 22878 water molecules. The system was neutralized by Na^+ and Cl^- resulting in a system with a net charge of zero. Simulation system was performed at 298 K, pH 7.4 for 20 ns. The simulation snapshots were capture every 500 ps. GROMACS tools and YASARA "md_analyze.mcr" macro were utilized for trajectory analysis.

Substrate binding assay by UV/Vis spectroscopy

The determination is modified by protocol of Bernhardt et. al.[34] The substrate binding assay was carried out at room temperature using an UV/Vis spectroscopy (Varian Cary 50 UV-Vis, USA) in a 1 cm path-length cuvette. The reaction mixture contained 3 μM purified P450 BM3 monooxygenase in 1 mL KPi (50 mM, pH 7.4). The titration was carried out by adding small aliquot of α-isophorone, and the spectra were recorded. The main Soret absorption band is from 420 nm 390 nm. The dissociation constant (K_d) was determined by fitting Equation (1):

$$(\Delta A_{390}\text{-}\Delta A_{420}) = (\Delta A_{390}-\Delta A_{420})_{max}/2E) \times \{(K_d + E + S) - [(K_d + E + S)^{2-} 4ES]^{1/2}\} \quad (1)$$

where E is the P450 BM3 concentration and S is the substrate concentration. All reactions were performed in triplicate. Data were fitted by nonlinear fitting model using OriginPro 9.1.0 software (OriginLab Corporation, Northampton, MA, USA).

Acknowledgements

Shuaiqi Meng was supported by a Ph.D. scholarship from the China Scholarship Council (CSC No. 201906880011). The authors thank Dr. Anna Joëlle Ruff for providing experimental support. Open Access funding enabled and organized by Projekt DEAL.

Conflict of Interest

The authors declare no conflict of interest.

Data Availability Statement

The data that support the findings of this study are available from the corresponding author upon reasonable request.

Keywords: biocatalysis · cytochrome P450 · directed evolution · hydrophobicity · protein engineering

[1] a) X. Zhang, S. Li, *Nat. Prod. Rep.* **2017**, *34*, 1061–1089; b) W. Zhang, Y. Liu, J. Yan, S. Cao, F. Bai, Y. Yang, S. Huang, L. Yao, Y. Anzai, F. Kato, L. M. Podust, D. H. Sherman, S. Li, *J. Am. Chem. Soc.* **2014**, *136*, 3640–3646.
[2] a) J. Caswell, M. O'Neill, S. Taylor, T. Moody, *Curr. Opin. Chem. Biol.* **2013**, *17*, 271–275; b) V. B. Urlacher, M. Girhard, *Trends Biotechnol.* **2012**, *30*, 26–36.
[3] a) H. M. Girvan, A. W. Munro, *Curr. Opin. Chem. Biol.* **2016**, 136–145; b) Y. V. Grinkova, I. G. Denisov, M. A. McLean, S. G. Sligar, *Biochem. Biophys. Res. Commun.* **2013**, *430*, 1223–1227.
[4] D. Darimont, M. J. Weissenborn, B. A. Nebel, B. Hauer, *Bioelectrochemistry* **2018**, *119*, 119–123.
[5] a) S. T. Jung, R. Lauchli, F. H. Arnold, *Curr. Opin. Biotechnol.* **2011**, *22*, 809–817; b) M. Dietrich, T. A. Do, R. D. Schmid, J. Pleiss, V. B. Urlacher, *J. Biotechnol.* **2009**, *139*, 115–117.
[6] a) E. T. Farinas, M. Alcalde, F. Arnold, *Tetrahedron* **2004**, *60*, 525–528; b) G. A. Santos, G. V. Dhoke, M. D. Davari, A. J. Ruff, U. Schwaneberg, *Int. J. Mol. Sci.* **2019**, *20*; c) Y. Ji, A. M. Mertens, C. Gertler, S. Fekiri, M. Keser, D. F. Sauer, K. E. C. Smith, U. Schwaneberg, *Chem. Eur. J.* **2018**, *24*, 16865–16872.
[7] L. C. Seaver, J. A. Imlay, *J. Biol. Chem.* **2004**, *279*, 48742–48750.
[8] S. M. Hoffmann, M. J. Weissenborn, Ł. Gricman, S. Notonier, J. Pleiss, B. Hauer, *ChemCatChem* **2016**, *8*, 1591–1597.
[9] P. J. Loida, S. G. Sligar, *Biochemistry* **1993**, *32*, 11530–11538.
[10] C. J. Whitehouse, S. G. Bell, L. L. Wong, *Chem. Soc. Rev.* **2012**, *41*, 1218–1260.
[11] N. Shakunthala, *Expert Opin. Drug Metab. Toxicol.* **2010**, *6*, 1–15.
[12] R. Raag, T. L. Poulos, *Biochemistry* **1991**, *30*, 2674–2684.
[13] P. Bracco, H. J. Wijma, B. Nicolai, J. A. Rodriguez Buitrago, T. Klünemann, A. Vila, P. Schrepfer, W. Blankenfeldt, D. B. Janssen, A. Schallmey, *ChemBioChem* **2020**, *22*, 1099–1110.
[14] a) V. Cojocaru, P. J. Winn, R. C. Wade, *Biochim. Biophys. Acta* **2007**, *1770*, 390–401; b) S. Meng, R. An, Z. Li, U. Schwaneberg, Y. Ji, M. D. Davari, F. Wang, M. Wang, M. Qin, K. Nie, L. Liu, *BioResources* **2021**, *8*; c) L. R. Rapp, S. M. Marques, E. Zukic, B. Rowlinson, M. Sharma, G. Grogan, J. Damborsky, B. Hauer, *ACS Catal.* **2021**, *11*, 3182–3189.
[15] N. Kress, J. M. Halder, L. R. Rapp, B. Hauer, *Curr. Opin. Chem. Biol.* **2018**, *47*, 109–116.
[16] a) M. Tavanti, F. Parmeggiani, J. R. G. Castellanos, A. Mattevi, N. J. Turner, *ChemCatChem* **2017**, *9*, 3338–3348; b) M. Eggersdorfer, D. Laudert, U. Letinois, T. McClymont, J. Medlock, T. Netscher, W. Bonrath, *Angew. Chem. Int. Ed.* **2012**, *51*, 12960–12990; *Angew. Chem.* **2012**, *124*, 13134–13165.
[17] J. Stourac, O. Vavra, P. Kokkonen, J. Filipovic, G. Pinto, J. Brezovsky, J. Damborsky, D. Bednar, *Nucleic Acids Res.* **2019**, *47*, W414–W422.
[18] A. Gärtner, PhD thesis, RWTH Aachen, **2020**.
[19] H. Cui, H. Cao, H. Cai, K. E. Jaeger, M. D. Davari, U. Schwaneberg, *Chem. Eur. J.* **2020**, *26*, 643–649.
[20] I. F. Sevrioukova, H. Li, H. Zhang, J. A. Peterson, T. L. Poulos, *Proc. Nat. Acad. Sci.* **1999**, *96*, 1863–1868.
[21] L. Chen, R. Tang, Z. Li, S. Liang, *Bull. Korean Chem. Soc.* **2012**, *33*, 459–463.

© 2021 The Authors. ChemSusChem published by Wiley-VCH GmbH

[22] R. A. Luirink, S. J. Dekker, L. Capoferri, L. F. H. Janssen, C. L. Kuiper, M. E. Ari, N. P. E. Vermeulen, J. C. Vos, J. N. M. Commandeur, D. P. Geerke, *J. Inorg. Biochem.* **2018**, *184*, 115–122.
[23] a) D. Sehnal, R. S. Vařeková, K. Berka, L. Pravda, V. Navrátilová, P. Banáš, C.-M. Ionescu, M. Otyepka, J. Koča, *J. Cheminf.* **2013**, *5*, 39; b) L. Pravda, D. Sehnal, D. Tousek, V. Navratilova, V. Bazgier, K. Berka, R. Svobodova Varekova, J. Koca, M. Otyepka, *Nucleic Acids Res.* **2018**, *46*, W368-W373.
[24] J. Zimmerman, N. Eliezer, R. Simha, *J. Theor. Biol.* **1968**, *21*, 170–201.
[25] P. J. Mak, I. G. Denisov, *Biochim. Biophys. Acta* **2018**, *1866*, 178–204.
[26] J. Nazor, U. Schwaneberg, *ChemBioChem* **2006**, *7*, 638–644.
[27] U. Schwaneberg, A. Sprauer, C. Schmidt-Dannert, R. Schmid, *J. Chromatogr. A* **1999**, *848*, 149–159.
[28] T. Omura, R. Sato, *J. Biol. Chem.* **1964**, *239*, 2370–2378.
[29] H. Land, M. S. Humble, *Methods Mol. Biol.* **2018**, *1685*, 43–67.
[30] a) H. Ashkenazy, S. Abadi, E. Martz, O. Chay, I. Mayrose, T. Pupko, N. Ben-Tal, *Nucleic Acids Res.* **2016**, *44*, W344–350; b) G. Celniker, G. Nimrod, H. Ashkenazy, F. Glaser, E. Martz, I. Mayrose, T. Pupko, N. Ben-Tal, *Isr. J. Chem.* **2013**, *53*, 199–206; c) H. Ashkenazy, E. Erez, E. Martz, T. Pupko, N. Ben-Tal, *Nucleic Acids Res.* **2010**, *38*, W529–533.
[31] *Amber 14*, D. A. Case, V. Babin, J. Berryman, R. M. Betz, Q. Cai, D. S. Cerutti, T. E. Cheatham III, T. A. Darden, R. E. Duke, H. Gohlke, A. W. Goetz, S. Gusarov, N. Homeyer, P. Janowski, J. Kaus, I. Kolossváry, A. Kovalenko, T. S. Lee, S. LeGrand, T. Luchko, R. Luo, B. Madej, K. M. Merz, F. Paesani, D. R. Roe, A. Roitberg, C. Sagui, R. Salomon-Ferrer, G. Seabra, C. L. Simmerling, W. Smith, J. Swails, R. C. Walker, J. Wang, R. M. Wolf, X. Wu, P. A. Kollman, **2014**, http://hdl.handle.net/10993/16614.
[32] J. Wang, R. M. Wolf, J. W. Caldwell, P. A. Kollman, D. A. Case, *J. Comput. Chem.* **2004**, *25*, 1157–1174.
[33] A. Jakalian, D. B. Jack, C. I. Bayly, *J. Comput. Chem.* **2002**, *23*, 1623–1641.
[34] Y. Khatri, M. Girhard, A. Romankiewicz, M. Ringle, F. Hannemann, V. B. Urlacher, M. C. Hutter, R. Bernhardt, *Appl. Microbiol. Biotechnol.* **2010**, *88*, 485–495.

Manuscript received: November 15, 2021
Revised manuscript received: December 19, 2021
Accepted manuscript online: December 22, 2021
Version of record online: January 27, 2022

© 2021 The Authors. ChemSusChem published by Wiley-VCH GmbH